

Manganese(II) and zinc(II) complexes of 4-phenyl (2-methoxybenzoyl)-3-thiosemicarbazide: Synthesis, spectral, structural characterization, thermal behavior and DFT study



A. Singh^a, M.K. Bharty^{a,*}, R.K. Dani^a, Sanjay Singh^b, S.K. Kushawaha^a, N.K. Singh^{a,*}

^a Department of Chemistry, Banaras Hindu University, Varanasi 221 005, India

^b Department of Chemical Science IISER-Mohali, Knowledge City, Sector 81, S.A.S Nagar, Mohali 140306, Punjab, India

ARTICLE INFO

Article history:

Received 23 October 2013

Accepted 13 February 2014

Available online 26 February 2014

Keywords:

Thiosemicarbazide

Mn(II) and Zn(II) complexes

Crystal structure

Supramolecular architecture

DFT

TGA

ABSTRACT

The ligand 4-phenyl(2-methoxybenzoyl)-3-thiosemicarbazide (Hpmt), forms isostructural [Mn(pmt)₂(*o*-phen)] (**1**) and [Zn(pmt)₂(*o*-phen)] (**2**) complexes containing *o*-phen as coligand which have been characterized by analytical, spectroscopic (IR, UV–Vis, NMR), magnetic susceptibility, TGA and single crystal X-ray data. Both complexes crystallize in monoclinic systems with the space group *P2*/*n*. The complexes have distorted octahedral geometry around the metal center. The ligand in the complexes is coordinated through the deprotonated hydrazinic nitrogen and carbonyl oxygen. The hydrazinic nitrogen coordinates with a shorter M–N distance than the *o*-phen nitrogen and bond lengths in the chelate ring systems are intermediate between single and double bond distances, suggesting considerable delocalization of charge. There is a good agreement between the geometrical parameters obtained by X-ray crystallography to those generated by DFT method. The thermal degradations of complexes **1** and **2** have been investigated by thermogravimetric analyses which indicate that the final residues left are Mn(NCO)₂ and Zn(NCSNH)₂. The small HOMO–LUMO energy gap suggests low excitation energy for the complexes.

© 2014 Elsevier Ltd. All rights reserved.

1. Introduction

Thiosemicarbazide is the simplest representative of the ligands having nitrogen and sulfur as donors. Thiosemicarbazide and substituted thiosemicarbazides are an important class of intermediate used for the synthesis of five membered nitrogen–sulfur or nitrogen–oxygen heterocyclic compounds [1–3]. The chemistry of thiosemicarbazide/ substituted thiosemicarbazide complexes has received much attention owing to their significant biological and medicinal properties which are dependent upon the chemical nature of the moiety attached to the C=S carbon atom [4–7]. 1,4-Disubstituted-thiosemicarbazide are biologically versatile compounds displaying a variety of biological effects which include anti-inflammatory [8], antimycobacterial [9,10], antimicrobial [11–13], antifungal [14], antibacterial [15,16] and antiviral [10] activities. Metal complexes containing 1,10-phenanthroline and bipyridine have gained importance because of their versatile roles as building blocks for the synthesis of metallo-dendrimers and as molecular scaffolding for supramolecular assemblies, and in

analytical chemistry, catalysis, electrochemistry, ring-opening metathesis polymerization and biochemistry [17–23]. However, most diimine complexes reported are homo ligand compounds of the general formula [M(N–N)₃]ⁿ⁺ or [M(N–N)₂(NCS)₂] which have shown variable spin transition properties with temperature [24]. Mixed ligand complexes can be a synthetic challenge to tune the various properties of the transition metal complexes. A few papers are available on the transition metal complexes of 1,4-substituted thiosemicarbazide [25,26] but there is no report on the synthesis and structural characterization of the mixed ligand complexes containing bidentate N,N donors and 1,4-disubstituted thiosemicarbazide. In this paper, we report the synthesis and structural characterization of Mn(II) and Zn(II) complexes of 4-phenyl(2-methoxybenzoyl)-3-thiosemicarbazide and the DFT calculations have been done to corroborate the structural data.

2. Experimental

2.1. Chemical and starting materials

Commercial reagents were used without further purification and all experiments were carried out in open atmosphere. Phenyl isothiocyanate, methyl-2-methoxy benzoate (Sigma Aldrich),

* Corresponding authors. Tel.: +91 5426702452; fax: +91 5422368127.

E-mail addresses: manoj_vns2005@yahoo.co.in (M.K. Bharty), singhmk_bhu@yahoo.com (N.K. Singh).

hydrazine hydrate (SD Fine) were used as received. 2-Methoxy benzoic acid hydrazide was prepared by reported method [27]. All the synthetic manipulations were carried out in open atmosphere and at room temperature. The solvents were dried and distilled before use following the standard procedure.

2.2. Physical measurements

Carbon, hydrogen and nitrogen contents were estimated on a CHN Model CE-440 Analyser and on an Elementar Vario EL III Carlo Erba 1108. Magnetic susceptibility measurements were performed at room temperature on a Cahn Faraday balance using Hg[Co(NCS)₄] as the calibrant and electronic spectra were recorded on a SHIMADZU 1700 UV-Vis spectrophotometer. IR spectra were recorded in the 4000–400 cm⁻¹ region as KBr pellets on a Varian Excalibur 3100 FT-IR spectrophotometer. ¹H and ¹³C NMR spectra were recorded in DMSO-d₆ on a JEOL AL300 FT NMR spectrometer using TMS as an internal reference. Thermogravimetric analyses (TG-DTA) of the compounds were performed on a Perkin Elmer STA 6000 thermal analyzer at a heating rate of 5 °C/min in N₂ atmosphere.

2.3. X-ray crystallography

Crystals suitable for X-ray analyses of complexes **1** and **2** were grown at room temperature. X-ray diffraction data were obtained at 293(2)K on an Oxford Diffraction Gemini diffractometer equipped with CRYSLIS PRO., using a graphite mono-chromated Mo K α ($\lambda = 0.71073$ Å) radiation source. A semi-empirical multi scan absorption correction was applied to the X-ray data of both compounds. The structure was solved by direct methods (SHELXL-13) and refined by full matrix least-square on F^2 (SHELXL) using anisotropic displacement parameters for all non-hydrogen atoms. All hydrogen atoms were included in calculated position and refined with a riding model [28]. Figures were drawn using the programs MERCURY and ORTEP-3 [29,30].

2.4. Synthesis

2.4.1. Preparation of 4-phenyl(2-methoxybenzoyl)-3-thiosemicarbazide (Hpmt)

The ligand 4-phenyl(2-methoxybenzoyl)-3-thiosemicarbazide (Hpmt) was prepared as reported in literature [31].

2.4.2. Preparation of [Mn(pmt)₂(*o*-phen)] (**1**)

Methanolic solutions of Mn(OAc)₂·4H₂O (0.246 g, 1 mmol) and Hpmt (0.6 g, 2 mmol) were mixed and continuously stirred for 30 min at room temperature. The resulting white precipitate was filtered off, washed with ethanol and air dried. The precipitate was suspended in methanol and stirred with a methanol solution of 1,10-phenanthroline (0.2 g, 1 mmol). The resulting clear yellow solution was filtered off and kept for crystallization, which resulted after slow evaporation of the above solution over a period of 20 days, yellow rod shaped crystals of complex suitable for X-ray analyses. Yield: 70%. M.p: 498 K. Anal. Calc. for C₄₂H₃₆MnN₈O₄S₂ (835.87): C, 60.29; H, 4.30; N, 13.39; S, 7.65. Found: C, 60.25; H, 4.35; N, 13.28; S, 7.6%. IR data (ν cm⁻¹, KBr): 3272s ν (NH); 1594s thioamide I [β (NH) + ν (CN)]; 1346 thioamide II [ν (CN) + β (NH)]; 1018 ν (N–N) s; 1604 ν (C=O); 928 ν (C=S). UV-Vis [λ_{\max} , Nujol mulls, nm]: 280, 310, 648.

2.4.3. Preparation of [Zn(pmt)₂(*o*-phen)] (**2**)

Methanolic solution of Zn(OAc)₂·2H₂O (0.218 g, 1 mmol) was added to the methanolic solution of Hpmt (0.6 g, 2 mmol) and the reaction mixture was stirred continuously at room temperature for 30 min. The resulting white precipitate was filtered off,

washed with ethanol and air dried. The precipitate was suspended in methanol and stirred with a methanol solution of 1,10-phenanthroline (0.200 g, 1 mmol) at the room temperature which resulted in a clear yellow solution. This was filtered off and kept for crystallization. Yellow needle shaped crystals of the complex suitable for an X-ray analyses were obtained by slow evaporation of the above solution over a period of 10 days. Yield: 70%. M.p: 508 K. Anal. Calc for C₄₂H₃₆ZnN₈O₄S₂ (711.61): C, 59.52; H, 4.25; N, 13.23; S, 7.56. Found: C, 59.54; H, 4.24; N, 13.23; S, 7.25%. IR data (ν cm⁻¹, KBr): 3259s ν (NH); 1566 thioamide I [β (NH) + ν (CN)] s; 1351 thioamide II [ν (CN) + β (NH)] s; 1018 ν (N–N) s; 1586 ν (C=O); 930 ν (C=S). ¹H NMR (300 MHz, DMSO-d₆; δ ppm): 9.00 (s, 1H, NH); 8.58 (s, 1H, NH); 6.87–8.05 (aromatic protons); 3.87 (m, 3H, –OCH₃). The ¹³C NMR (DMSO-d₆; δ ppm): 177.66 (C=S), 152.66 (C=O), 116.93–130.75 (aromatic ring carbons), 65.39 (–OCH₃). UV-Vis [λ_{\max} , Nujol mulls, nm]: 325, 350.

3. Results and discussion

The ligand 4-phenyl(2-methoxybenzoyl)-3-thiosemicarbazide react with Mn(OAc)₂·4H₂O and Zn(OAc)₂·2H₂O and then with *o*-phen in methanol solution yielding [Mn(pmt)₂(*o*-phen)] (**1**) and [Zn(pmt)₂(*o*-phen)] (**2**), respectively. In both the complexes, the metal is bonded through deprotonated thiohydrazide nitrogen and carbonyl oxygen of the ligand. The six coordination of Mn(II) and Zn(II) is completed by coordination of one molecule of *o*-phen and two molecules of the ligand. These complexes are stable toward air and moisture. Scheme 1 depicts the formation of the ligand and complexes containing *o*-phen as co-ligand. The complexes **1** and **2** are soluble in chloroform and melt at 498 and 508 K, respectively.

3.1. IR spectra

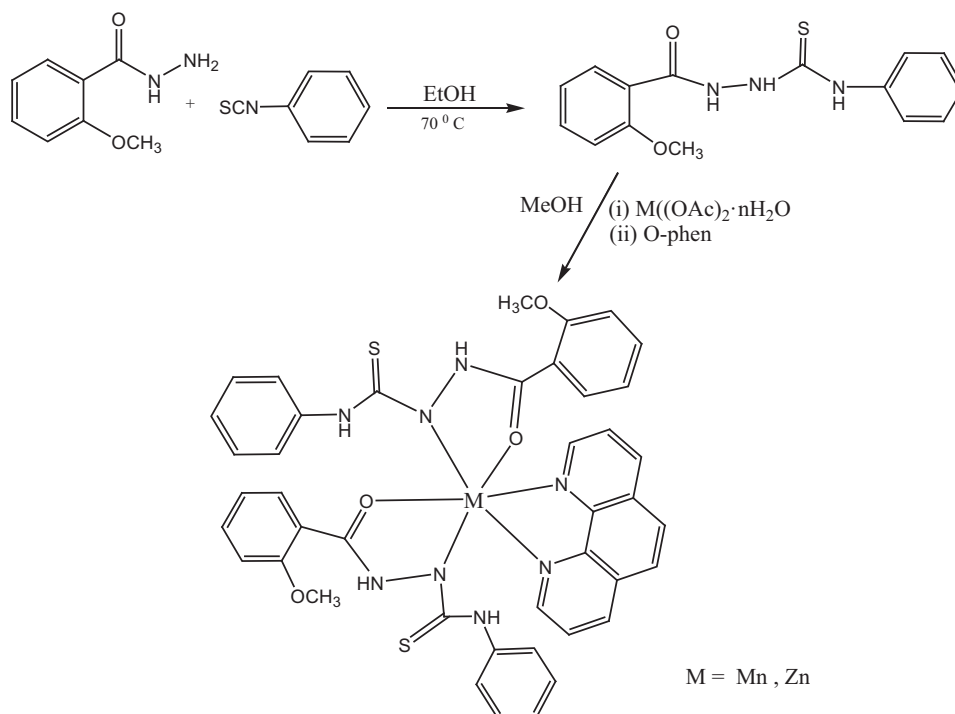
Complexes **1** and **2** show the absence of ν (N–H) band at 3201 cm⁻¹ indicating loss of hydrogen from the nitrogen of thiohydrazide group which is supported by a small positive shift of 13 cm⁻¹ in ν (N–N). The IR spectra of complexes **1** and **2** show a negative shift of 48–68 cm⁻¹ in ν (C=O) indicating bonding of the carbonyl oxygen to the metal ion. Furthermore, complexes **1** and **2** show a very small positive shift in ν (C=S) as compared to the free ligand, showing that the thiohydrazide sulfur is not participating in bonding but the small positive shift can be attributed to the involvement of sulfur in hydrogen bonding with the hydrogen of *o*-phen. Thus, it is clear from the IR data that the ligand acts as uninegative bidentate in complexes **1** and **2** bonding through deprotonated thiohydrazide nitrogen and carbonyl oxygen [32].

3.2. Electronic spectra and magnetic moments

The magnetic moment value of 5.85 B.M. for [Mn(pmt)₂(*o*-phen)] (**1**) suggests the presence of high spin Mn(II) with five unpaired electrons. The electronic spectrum of **1** shows a band at 648 nm which may be assigned to the ⁶A_{1g} → ⁴T_{1g} transition in an octahedral geometry [33]. Other high energy bands in complex **1** occurring at 280 and 310 nm are due to π → π^* and n → π^* transitions, respectively. [Zn(pmt)₂(*o*-phen)] (**2**) is diamagnetic and shows two high intensity bands at 325 and 350 nm due to π → π^* and n → π^* transitions, respectively.

3.2.1. ¹H and ¹³C NMR spectra

The ¹H NMR spectrum of [Zn(pmt)₂(*o*-phen)] (**2**) shows two signals at 9.00 (s, 1H) and 8.58 (s, 1H, NH) ppm due to the proton of NH group attached to carbonyl and phenyl group, respectively. The methoxy hydrogens appear at 3.87 ppm. Phenyl and *o*-phen ring



Scheme 1. Syntheses of Mn(II) and Zn(II) complexes.

protons appear as multiplet between δ 6.87–8.05 ppm. The ^{13}C spectrum of $[\text{Zn}(\text{pmt})_2(o\text{-phen})]$ (**2**) shows signals at δ 177.66, 152.66 and 65.39 ppm for (C=S), (C=O) and $-\text{OCH}_3$ carbons, respectively. The aromatic carbons appear between δ 116.93–130.75 ppm. A negative shift of 2.02 ppm in C=O and disappearance of one NH proton attached to C=S group suggests bonding through carbonyl oxygen and one thiohydrazide nitrogen after deprotonation.

3.3. Thermal gravimetric analysis

The thermal properties of complexes $[\text{Mn}(\text{pmt})_2(o\text{-phen})]$ (**1**) and $[\text{Zn}(\text{pmt})_2(o\text{-phen})]$ (**2**) were studied by TG and DTA in the temperature range 30–900 °C under a nitrogen atmosphere (Fig. 1). Thermogravimetric analysis of complexes **1** and **2** showed that the complexes start decomposing around 200 °C and thermograms exhibit four distinct decompositions at 200, 360, 550 and 700 °C for Mn(II) complex and at 200, 320, 410 and 720 °C for Zn(II) complex. The weight loss (6.162 for **1** and 7.02% for **2**) around 220 °C could be ascribed to the loss of $-\text{OCH}_3$ moiety and second

decompositions between 320–360 °C show the weight loss (24.31% for **1** and 24.52% for **2**) of *o*-phen from both the complexes. The third decomposition between 500 and 550 °C for complex **1**, corresponds to loss (52.28%) of two PhNHCSN moiety and the last decompositions between 600 and 700 °C show the degradation of the remaining organic moieties (17.24%) and finally $\text{Mn}(\text{NCO})_2$ is left as a residue. Whereas, the third decomposition for complex **2**, corresponds to loss (42.42%) of two PhCONH moiety between 410 and 450 °C and the last decompositions between 720 and 760 °C show the degradation of the remaining organic moieties (26.03%) and finally $\text{Zn}(\text{NCSNH})_2$ is left behind. The corresponding endo and exothermic peaks in DTA at 305, 360 and 470 and 810 °C for complex **1** and at 340, 480 and 540 and 800 °C for complex **2** were obtained.

3.4. Crystal structure description of complexes **1** and **2**

Figs. 5 and 7 show the ORTEP diagram of $[\text{Mn}(\text{pmt})_2(o\text{-phen})]$ (**1**) and $[\text{Zn}(\text{pmt})_2(o\text{-phen})]$ (**2**), respectively, together with the atomic numbering scheme. In both complexes, the metal ions,

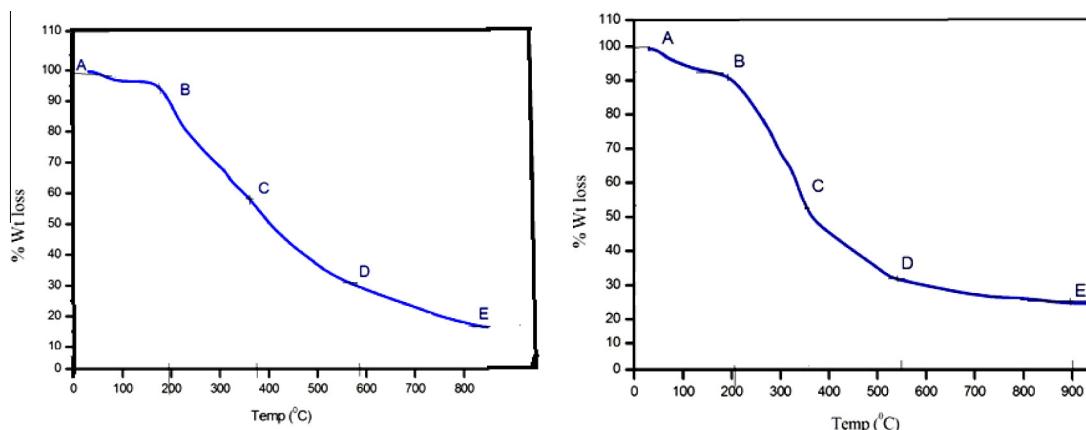


Fig. 1. Thermograms of $[\text{Mn}(\text{pmt})_2(o\text{-phen})]$ (**1**) and $[\text{Zn}(\text{pmt})_2(o\text{-phen})]$ (**2**).

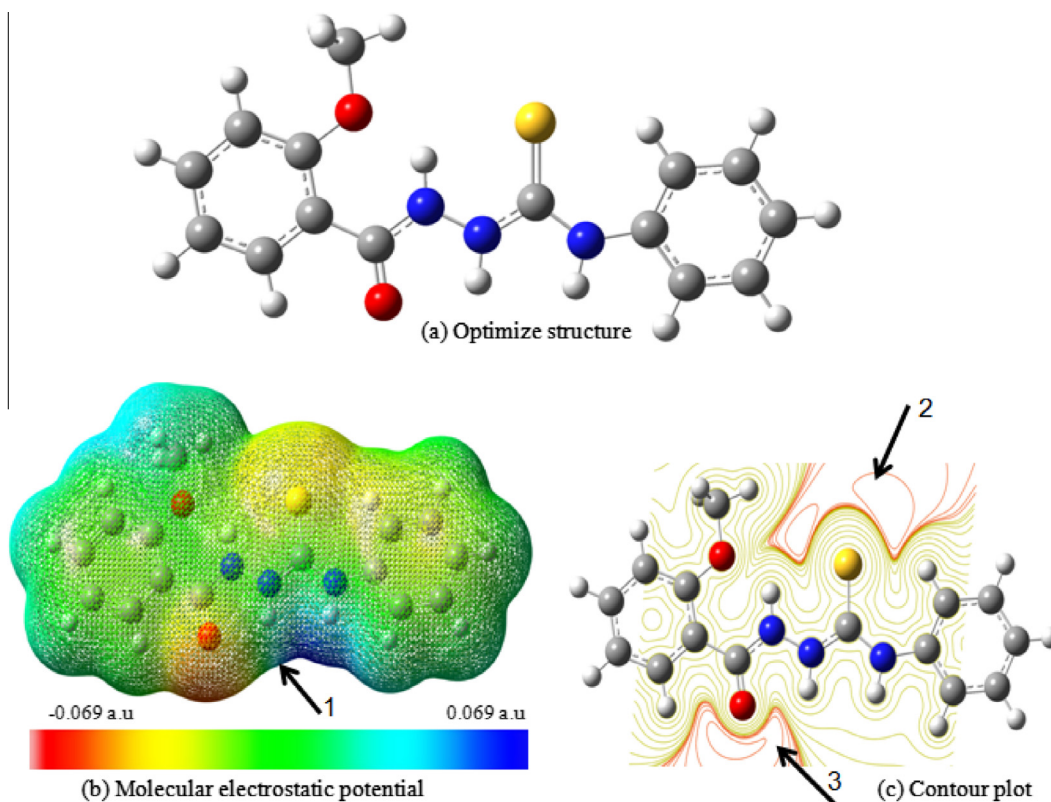


Fig. 2. Optimized structure (a), MEP (b) and contour plot (c) of ligand Hpmt.

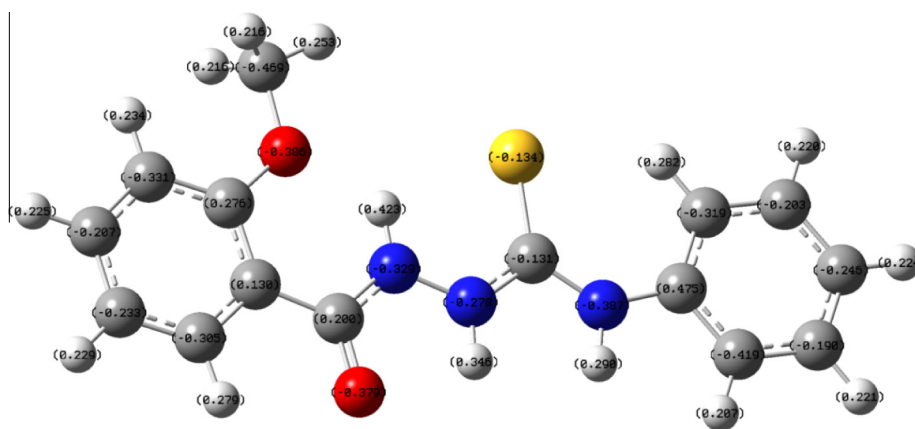


Fig. 3a. Charge distribution on atoms of Hpmt.

Zn(II) and Mn(II), possess distorted octahedral geometry. The crystallographic asymmetric units in the complexes $[\text{Mn}(\text{pmt})_2(o\text{-phen})]$ (**1**) and $[\text{Zn}(\text{pmt})_2(o\text{-phen})]$ (**2**), comprise of two complex molecules. The details of data collection, structure solution and refinement of complexes **1** and **2** are listed in Table 1. Some selected bond distances and bond angles in these structures are compiled in Tables 3 and 4. The metal center is coordinated in an N_4O_2 manner by two uninegative ligand moieties using pairs of hydrazine nitrogen, carbonyl oxygen and *o*-phen nitrogen; forming three five membered chelate rings. The carbon–sulfur bond length [1.680(2) Å] is purely a C=S double bond which remains uncoordinated and takes part in N–H \cdots S hydrogen bonding providing a supramolecular architecture. The hydrazine moiety, which connects two functional groups *viz.* carbo and thiocarbo involves the whole system in resonance. Consequently, N–N and C=O

distances are found to be intermediate between single and double-bond lengths indicating a delocalization of π -electrons. The average bond lengths N2–N1 = 1.388, N1–C7 = 1.323, N2–C8 = 1.342, C7–O1 = 1.266 Å for **1** and N1–N2 = 1.385, N1–C8 = 1.318, N2–C9 = 1.340, C8–O2 = 1.270 Å for **2**, suggest considerable delocalization of charge. The distances within the chelate rings are intermediate between single and double bond lengths as compared to the corresponding bond lengths in Hpmt. The bite angles 160.83(7) [N(2)–Mn(1)–N(4)] and 109.82(11)° [N(2)–Mn(1)–N(2)] for complex **1** and 164.28(4) [N(2)–Zn(1)–N(4)] and 103.39(14)° [N(2)–Zn(1)–N(2)] for complex **2** suggest substantial deviation from an octahedral geometry. In both the complexes hydrazine nitrogen bonds with a shorter M–N distance than the *o*-phen nitrogen which indicates that the hydrazinic nitrogen bonds more strongly than the *o*-phen nitrogens. The bond

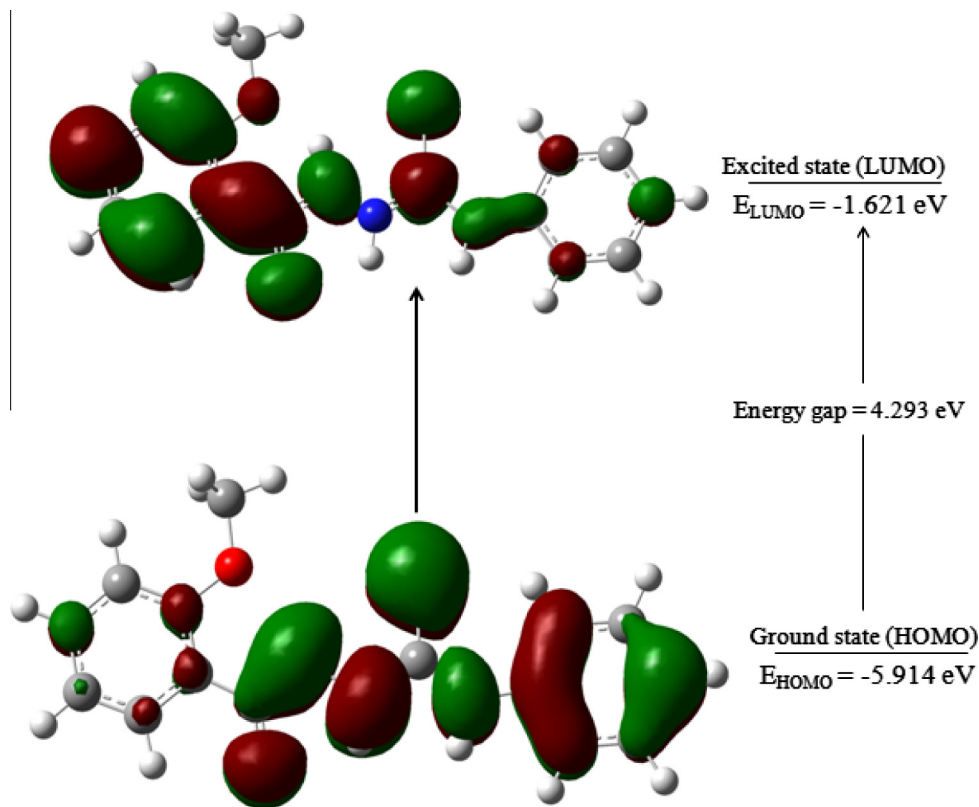


Fig. 4. Frontier molecular orbital diagrams of Hpmt.

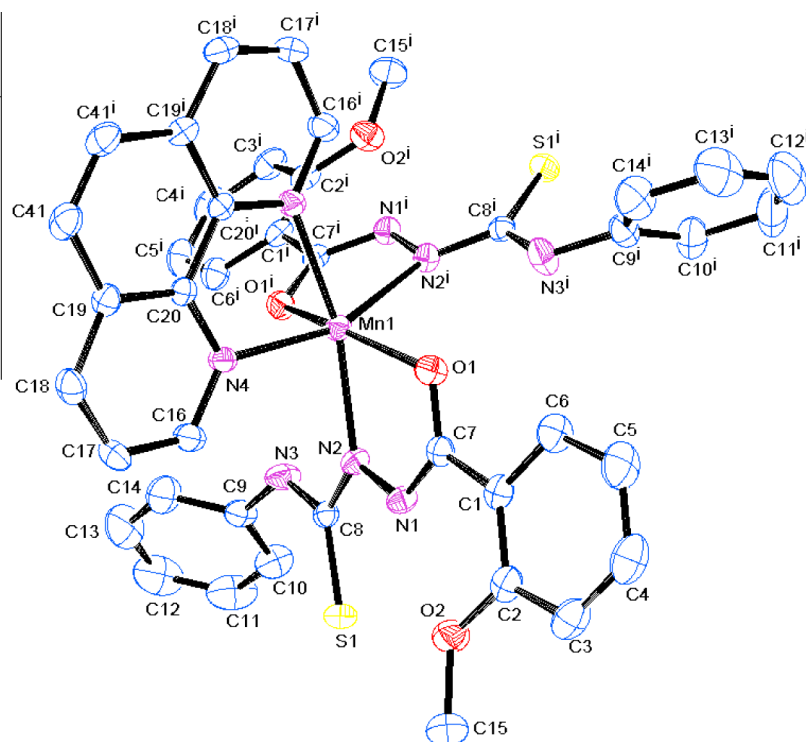


Fig. 5. ORTEP diagram of $[\text{Mn}(\text{pmt})_2(\text{o-phen})]$ (**1**) at 30% ellipsoids probability level. Hydrogen atoms are omitted for clarity.

intramolecular $\text{N-H}\cdots\text{O}$ hydrogen bonding occurring between hydrazinic hydrogen and carbonyl oxygen which was present in Hpmt is retained in complexes. The crystal structures of the

complexes **1** and **2** are stabilized through weak intramolecular $\text{N-H}\cdots\text{O}$ and $\text{N-H}\cdots\text{S}$ interactions formed between hydrazinic hydrogen and carbonyl oxygen/ thioamide sulfur producing

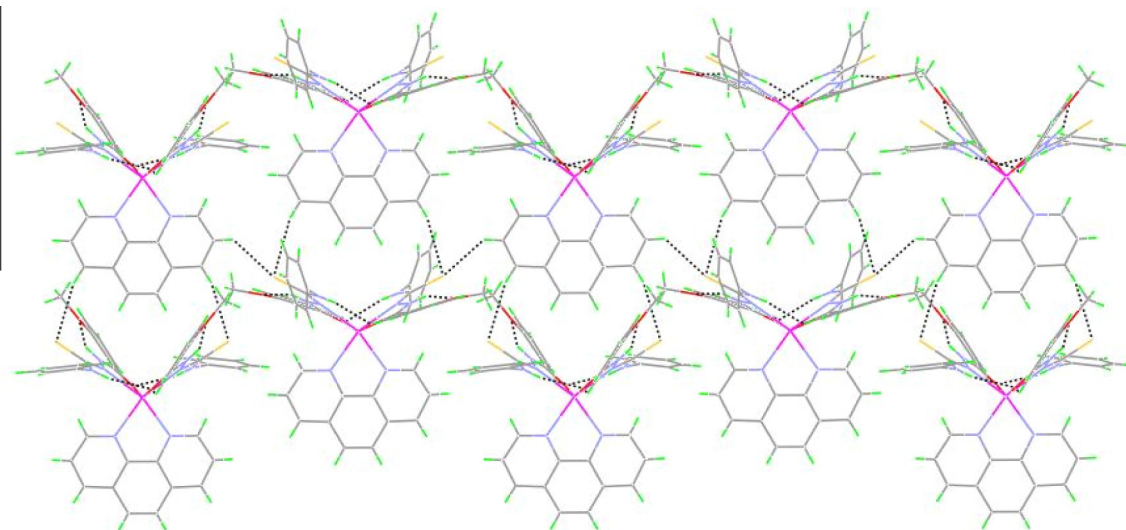


Fig. 6. N-H...O, C-H...S and C-H...O hydrogen bonds forming a sheet like structure in complex 2.

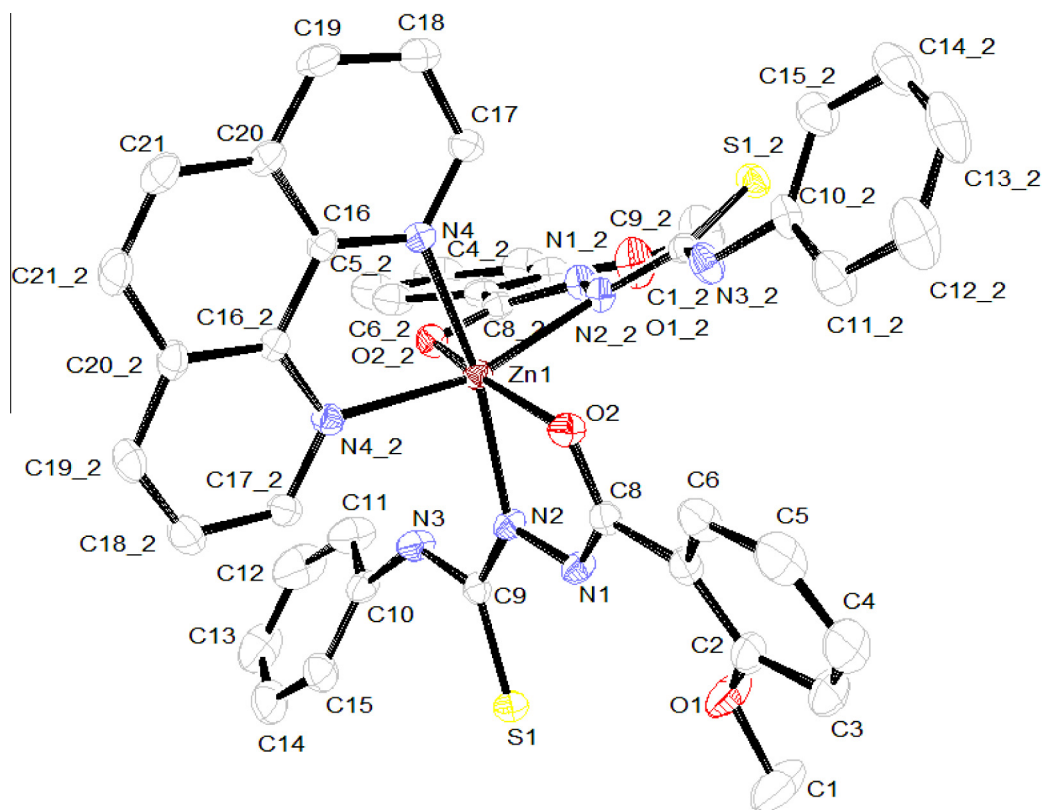


Fig. 7. ORTEP diagram of $[Zn(pmt)_2(o\text{-phen})]$ (**2**) at 30% ellipsoids probability level. Hydrogen atoms are omitted for clarity.

supramolecular architecture [Figs. 6 and 8]. Complexes **1** and **2** are further stabilized by intermolecular C-H...S interactions occurring between thioamide sulfur and hydrogens of *o*-phen ring (See Fig. 10).

3.5. DFT calculations of ligand Hpmt and its Mn(II) and Zn(II) complexes

All calculations for 4-phenyl(2-methoxybenzoyl)-3-thiosemicarbazide as well as its complexes with Mn(II) and Zn(II) have been

performed with GAUSSIAN 03 and GAUSS VIEW 4.1 [36] program packages. The structure optimization of 4-phenyl(2-methoxybenzoyl)-3-thiosemicarbazide have been done using DFT method with functional B3LYP and basis set 6-311G(d,p) whereas the geometry optimization for the Mn(II) and Zn(II) complexes have been done using basis sets LanL2DZ [37,38] which is most popular and serves the purpose of including the pseudopotential of the core electrons of the metal ions. The input geometry of the complexes for the DFT calculations was generated from single crystal X-ray data. The optimized energy of Hpmt and its complexes **1** and **2** were -905.290

Table 1
Crystallographic data for complexes **1** and **2**.

Parameters	1	2
Empirical formula	C ₄₂ H ₃₆ MnN ₈ O ₄ S ₂	C ₄₂ H ₃₆ ZnN ₈ O ₄ S ₂
Formula weight	835.87	846.32
Crystal system	monoclinic	monoclinic
Space group	<i>P2</i> / <i>n</i>	<i>P2</i> / <i>n</i>
<i>T</i> (K)	293(2)	293(2)
λ , Mo K α (Å)	0.71073	0.71073
<i>a</i> (Å)	20.5608(10)	20.2813(18)
<i>b</i> (Å)	10.3699(4)	10.3655(7)
<i>c</i> (Å)	21.1878(10)	21.1656(17)
β (°)	116.993(6)	116.924(10)
<i>V</i> (Å ³)	4025.4(3)	3967.3(5)
<i>Z</i>	4	4
ρ_{calc} (g/cm ³)	1.379	1.417
μ (mm ⁻¹)	0.485	0.778
<i>F</i> (000)	1732	2080
Crystal size (mm ³)	0.29 × 0.27 × 0.25	0.28 × 0.27 × 0.25
θ Range for data collections (°)	3.32–28.99	3.03–29.21
Index ranges	–24 ≤ <i>h</i> ≤ 28, –14 ≤ <i>k</i> ≤ 11, –28 ≤ <i>l</i> ≤ 28	–25 ≤ <i>h</i> ≤ 18, –13 ≤ <i>k</i> ≤ 11, –25 ≤ <i>l</i> ≤ 26
No. of reflections collected	10762	9117
No. of independent reflections (<i>R</i> _{int})	6191	6156
No. of data/restraints/parameters	10762/0/515	9117/0/515
Goodness-of-fit (GOF) on <i>F</i> ²	0.982	0.970
<i>R</i> ₁ ^a , <i>wR</i> ₂ ^b [<i>I</i> > 2 σ (<i>I</i>)]	0.0469, 0.0941	0.0453, 0.1056
<i>R</i> ₁ ^a , <i>wR</i> ₂ ^b (all data)	0.0849, 0.1134	0.0810, 0.1378
Largest difference in peak/hole (e Å ⁻³)	0.291, –0.414	0.276, –0.386

^a $R_1 = \sum ||F_o| - |F_c|| / \sum |F_o|$.^b $R_2 = [\sum w(|F_o|^2 - |F_c|^2)|^2 / \sum w|F_o|^2]^{1/2}$.**Table 2**
Interatomic distances (Å) and angles (°) for Hpmt.

Bond length (Å)	Bond angles (°)	
	(Exp.) ^a	(Cal.)
S(1)–C(7)	1.667(2)	1.738
N(1)–C(8)	1.329(3)	1.371
C(7)–N(3)	1.350(3)	1.383
N(2)–C(7)	1.344(3)	1.371
O(1)–C(8)	1.238(1)	1.275
N(1)–N(2)	1.365(3)	1.391
C(8)–N(1)–N(2)	120.2(2)	116.81
C(7)–N(2)–N(1)	120.8(2)	122.64
O(1)–C(8)–N(1)	119.9(2)	119.27
N(2)–C(7)–S(1)	121.5(2)	120.74
C(9)–C(8)–O(1)	122.1(2)	122.66

^a Experimental data on bond length and bond angle of Hpmt given in Table 2 have been obtained from our own sample.**Table 3**
Interatomic distances (Å) and angles (°) for [Mn(pmt)₂(*o*-phen)] (**1**).

Mn1	Mn2	(Cal.)
<i>Bond lengths (Exp.)</i>		
S(1)–C(8)	1.690(2)	1.695(2)
N(2)–N(1)	1.393(2)	1.388(2)
N(2)–Mn(1)	2.219(2)	2.226(19)
C(7)–O(1)	1.263(3)	1.266(3)
N(2)–C(8)	1.334(3)	1.342(3)
N(1)–C(7)	1.323(3)	1.314(3)
Mn(1)–O(1)	2.155(15)	2.169(15)
Mn(1)–N(4)	2.288(2)	2.272(2)
<i>Bond angles (Exp.)</i>		
N(1)–N(2)–Mn(1)	109.25(13)	109.35(13)
O(1)–Mn(1)–O(1)	160.98(10)	155.83(9)
O(1)–Mn(1)–N(2)	74.12(6)	74.27(6)
O(1)–Mn(1)–N(2)	94.81(7)	91.35(6)
N(2)–Mn(1)–N(2)	109.82(11)	107.46(10)
O(1)–Mn(1)–N(4)	101.56(7)	99.27(6)
N(2)–Mn(1)–N(4)	89.02(7)	90.41(7)
N(4)–Mn(1)–N(4)	72.46(10)	72.81(10)
N(2)–Mn(1)–N(4)	160.83(7)	160.91(7)
S(2)–C(28)	1.695(2)	1.764
N(6)–N(5)	1.388(2)	1.403
N(6)–Mn(2)	2.226(19)	2.062
C(27)–O(3)	1.266(3)	1.318
N(6)–C(28)	1.342(3)	1.378
N(5)–C(29)	1.314(3)	1.335
Mn(2)–O(3)	2.169(15)	2.022
Mn(2)–N(8)	2.272(2)	2.018
N(5)–N(6)–Mn(2)	109.35(13)	109.08
O(3)–Mn(2)–O(3)	155.83(9)	166.62
O(3)–Mn(2)–N(6)	74.27(6)	80.10
O(3)–Mn(2)–N(6)	91.35(6)	80.10
N(6)–Mn(2)–N(6)	107.46(10)	96.63
O(3)–Mn(2)–N(8)	99.27(6)	93.06
N(6)–Mn(2)–N(8)	90.41(7)	92.01
N(8)–Mn(2)–N(8)	72.81(10)	81.09
N(6)–Mn(2)–N(8)	160.91(7)	167.25

(Hpmt), –2484.971 (Mn) and –2446.640 (Zn) a.u. respectively. The deviation in the geometrical parameters are due to the fact that the DFT calculations are done for an isolated molecule in gaseous phase while the X-ray crystallographic data were obtained from crystal lattice of complex molecules and shown in Tables 2–4. The optimized geometries of Hpmt and the complexes along with the atomic labeling scheme are shown in Fig. 2a and Fig. 9. From Mullikan charge distribution on atoms of Hpmt and its complexes (Figs. 3a–c), we observed that the charges on the ligand redistributed, as a result of complex formation. The charge on the carbonyl oxygen which is bonded to metal has lower value {–0.379 [ligand], –0.458 [Mn(II)] and –0.494 [Zn(II)]} whereas the charge on nitrogen which is bonded to metal has higher value{–0.278 [ligand], –0.227 [Mn(II)] and –0.212 [Zn(II)]}. The magnitude of the charges on carbon atoms was found to be either positive or negative.

3.6. Molecular electrostatic potential and contour maps

To predict reactive sites for electrophilic and nucleophilic processes for the Hpmt, electrostatic surface potentials were obtained at the B3LYP/6–311G(d,p) optimized geometry. The MEP mapped surface of the Hpmt and its complexes were calculated by DFT/B3LYP/6–311G(d,p){C,H,N,O,S}/LanL2DZ method at the 0.02 iso-values and 0.004 density values. The red color scheme of MEP is the negative electrostatic potentials. The red region show atoms with lone pairs; the intensity of the color is proportional to the absolute value of the potential energy. The positive electrostatic potentials are shown in blue color region which characterize the C–H bonds. The yellow/green areas cover parts of the molecule where electrostatic potentials are close to zero (C–C, C–N and C=S bonds). The MEP mapped surfaces are shown in Figs. 2b and 9. The different values of the electrostatic potential at the surface are represented by different colors. Potential increases in the order red < orange < yellow < green < blue. The color code of these maps is in the range of –0.069 to +0.069 a.u. for Hpmt, –0.061 to +0.061 a.u. for [Mn(pmt)₂(*o*-phen)] and –0.104 to +0.104 a.u. for [Zn(pmt)₂(*o*-phen)], where blue and red colors indicate the strongest attraction and repulsion, respectively. The negative red regions of MEP are related to electrophilic reactivity and the positive (blue) ones to nucleophilic reactivity. Negative (red) regions in the Hpmt were found around the carbonyl oxygen and positive regions (blue) are around H of hydrazinic nitrogens. Thus, it would be predicted that an electrophile would preferentially attack

Table 4
Interatomic distances (Å) and angles (°) for [Zn(pmt)₂(*o*-phen)] (**2**).

Zn1	Zn2	(Cal.)	
<i>Bond lengths (Exp.)</i>			
Zn(1)–O(2)	Zn(2)–O(4)	2.100(2)	2.115
Zn(1)–N(2)	Zn(2)–N(6)	2.130(3)	2.192
Zn(1)–N(4)	Zn(2)–N(8)	2.216(3)	2.379
S(1)–C(9)	S(2)–C(30)	1.699(3)	1.767
O(2)–C(8)	O(4)–C(29)	1.269(4)	1.312
N(1)–C(8)	N(5)–C(29)	1.318(4)	1.340
N(1)–N(2)	N(5)–N(6)	1.396(3)	1.399
N(2)–C(9)	N(6)–C(30)	1.329(4)	1.374
<i>Bond angles (Exp.)</i>			
O(2)–Zn(1)–O(2)	O(4)–Zn(2)–O(4)	168.70(13)	168.76
O(2)–Zn(1)–N(2)	O(4)–Zn(2)–N(6)	77.38(9)	76.73
N(2)–Zn(1)–N(2)	N(6)–Zn(2)–N(6)	106.66(14)	105.34
O(2)–Zn(1)–N(4)	O(4)–Zn(2)–N(8)	97.22(9)	91.91
N(2)–Zn(1)–N(4)	N(6)–Zn(2)–N(8)	163.47(10)	157.37
N(2)–Zn(1)–N(4)	N(6)–Zn(2)–N(8)	89.33(10)	88.14
O(2)–Zn(1)–N(4)	O(4)–Zn(2)–N(8)	91.75(9)	91.91
N(4)–Zn(1)–N(4)	N(8)–Zn(2)–N(8)	75.11(13)	73.70
N(1)–N(2)–Zn(1)	N(5)–N(6)–Zn(2)	108.41(18)	108.42
C(8)–O(2)–Zn(1)	C(29)–O(4)–Zn(2)	113.65(19)	114.24

to the ligand (Hpmt) at the O and N positions as indicated by arrow 1 (Fig. 2b). According to the calculated results, the MEP map shows that the negative potential sites are on electronegative oxygen atom as well as the positive potential sites are around the hydrogen atoms (more at hydrazinic moiety). These sites give information about the region from where the compound can have noncovalent interactions.

The contour maps are also calculated at same level of calculations of the MEP mapped surface of the Hpmt. The contour map of electrostatic potential is shown in Fig. 2c also confirms the different negative and positive potential sides of the Hpmt is in accordance with the molecular electrostatic potential. The red lines are around carbonyl oxygen, thione sulfur and methoxy oxygen side. But the attack of electrophile from thione sulfur and methoxy oxygen side is restricted due to crowd (shown by arrow 2) whereas

from carbonyl side no such crowd is observed (shown by arrow 3). Hence, the positive metal ions preferably bind through the carbonyl oxygen and hydrazinic nitrogen sides so that the negative potential shares with positive metal ion.

3.7. Frontier molecular orbital (FMO) analysis

The HOMO energy characterizes the ability of electron donation, the LUMO characterizes the ability of electron acceptance and the gap between HOMO and LUMO characterizes the molecular chemical stability [39]. The HOMO–LUMO energy and the energy gap (ΔE) for Hpmt and complexes have been calculated at DFT/B3LYP/6–311G(d,p) level. 3D plots of the HOMO and LUMO for Hpmt and complexes **1** and **2** are shown in Fig. 4 and 11, respectively. It can be seen that the HOMO orbital is located mainly at the HNCS moiety and phenyl ring of the Hpmt as a result of their electron withdrawing effect on the OCH₃ group, which in turn causes an increase in the LUMO electronic density as located on methoxy phenyl ring. Methoxy phenyl ring makes very little contribution to electronic density of HOMO, whereas in LUMO the phenyl ring does not make contribution to form frontier molecular orbitals. The values of the energy separation between the HOMO and LUMO are 4.293, 2.426 and 2.205 eV for Hpmt and complexes **1** and **2**, respectively. The small HOMO–LUMO energy gap means low excitation energy for the complexes, a good stability and a low chemical hardness for the complex. The electronic transition from the ground state to the excited state due to a transfer of electrons from the HOMO to LUMO level is mainly via $\pi \rightarrow \pi^*$ transition. The chemical hardness of a molecule is defined by the formula [39]

$$\eta = -E_{\text{HOMO}} + E_{\text{LUMO}}/2$$

where E_{HOMO} and E_{LUMO} are the energies of the HOMO and LUMO molecular orbitals. The value of η for Hpmt and complexes **1** and **2** are 2.146, 1.213 and 1.102 eV, respectively. The above result is supported by the presence of UV–Vis bands at 280 and 310 nm for complex **1** and at 325 and 350 nm for complex **2** which indicates that complex **2** is softer than complex **1**.

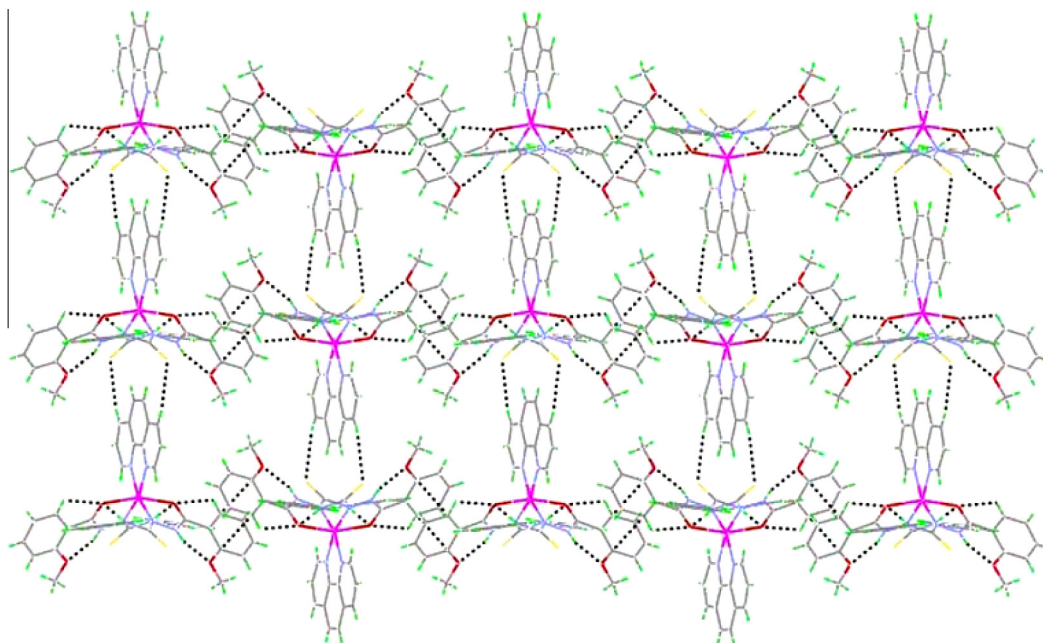


Fig. 8. N–H...O, C–H...O and C–H...S interactions forming a linear structure in complex **1**.

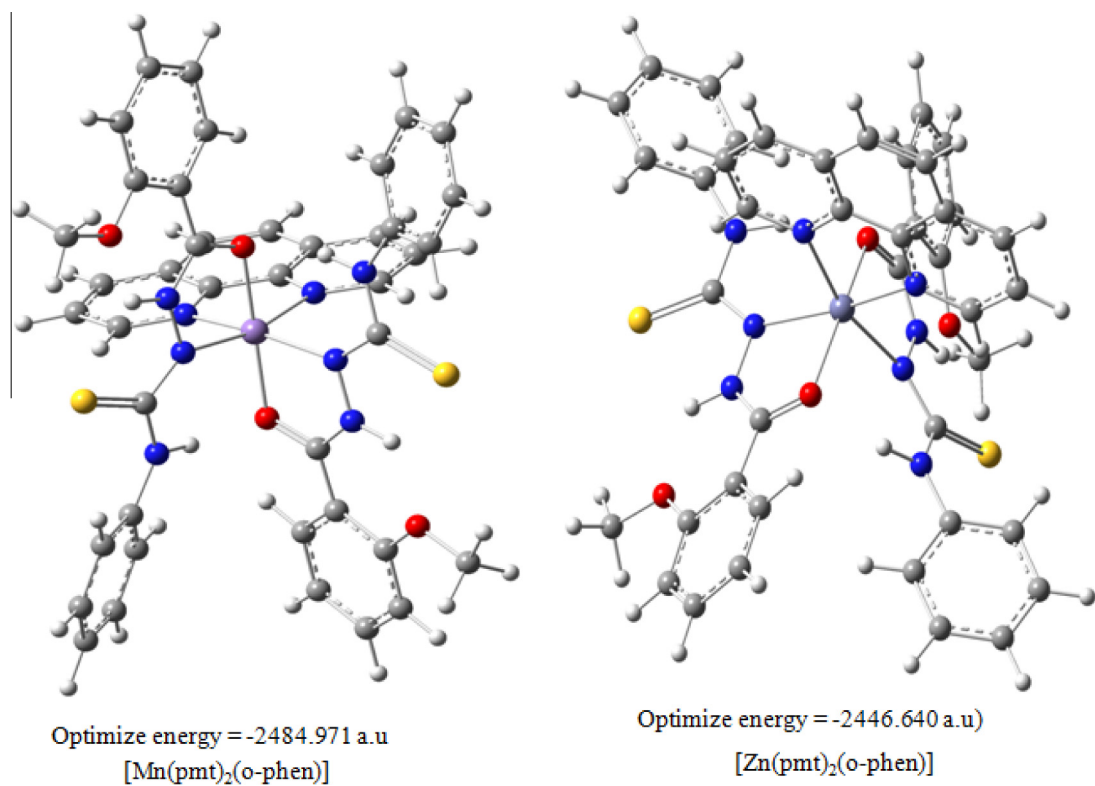


Fig. 9. Optimized structures of complexes 1 and 2.

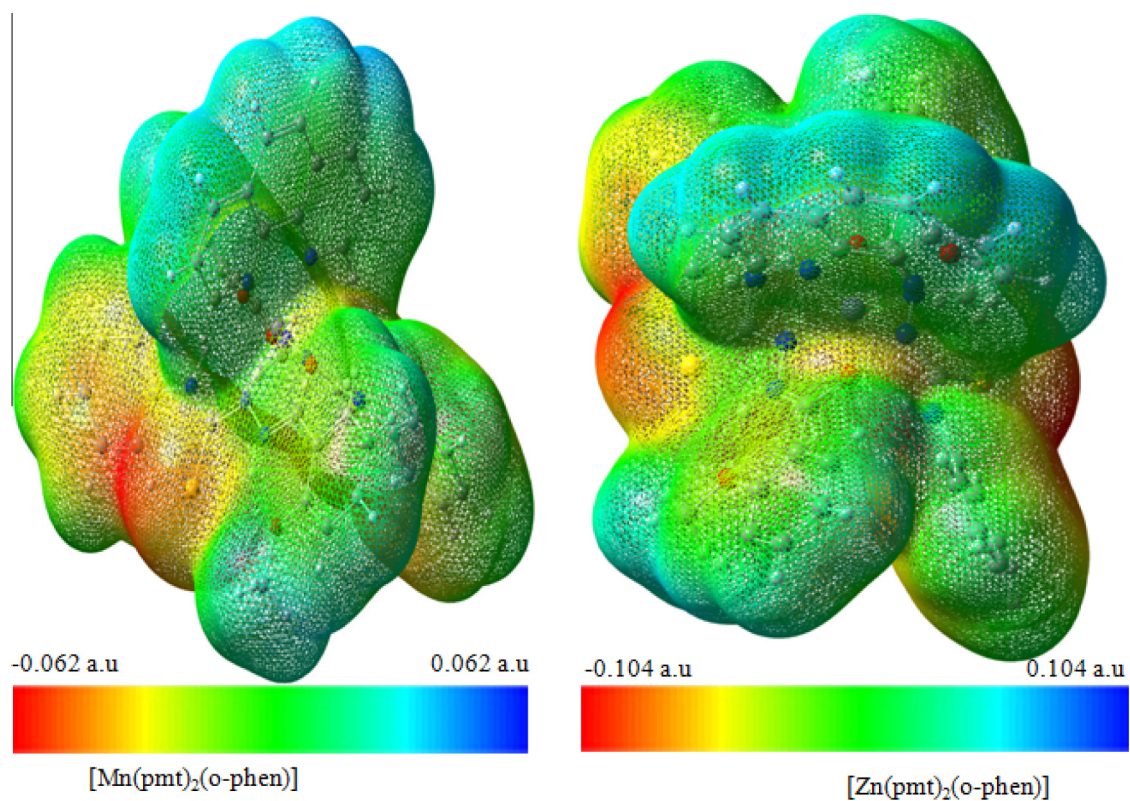


Fig. 10. MEP map of complexes 1 and 2.

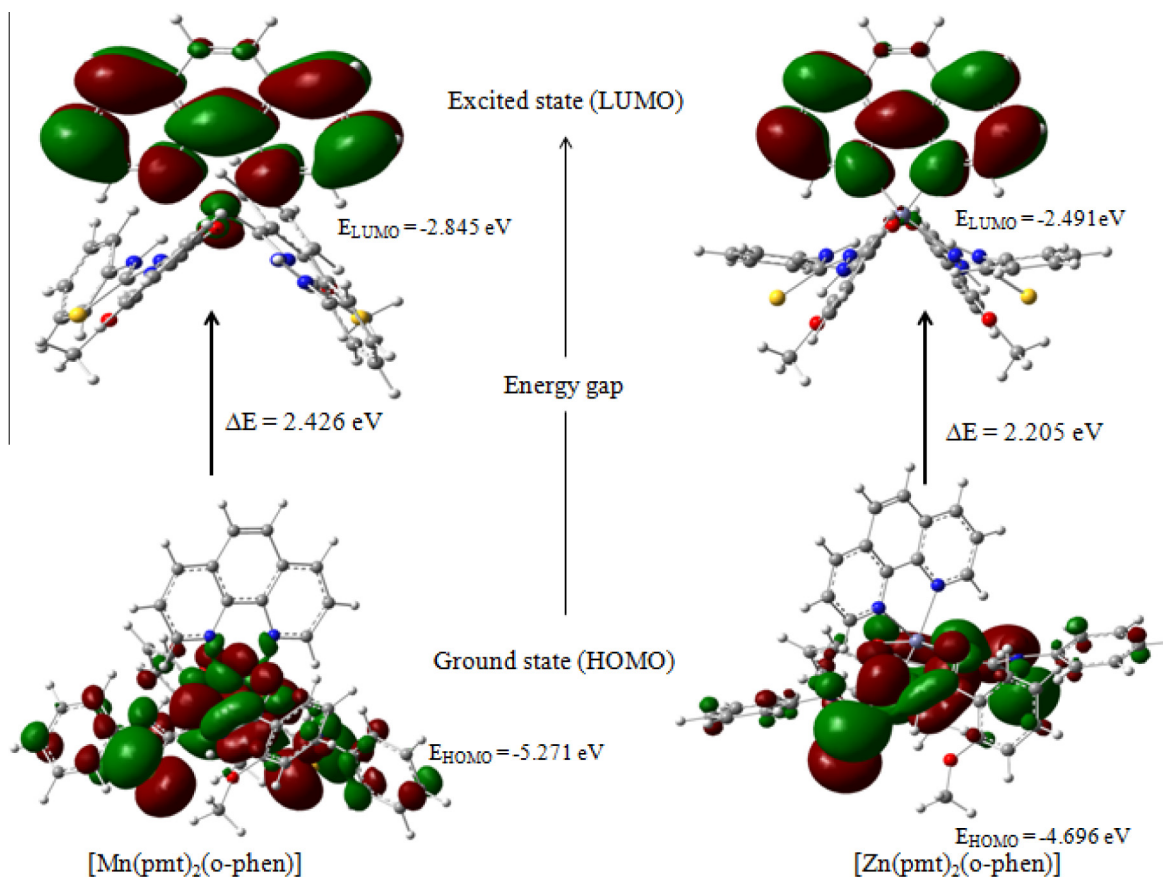


Fig. 11. FMO diagrams of complexes 1 and 2.

4. Conclusion

This paper reports the syntheses, spectral and crystal structure investigations of two new isostructural octahedral complexes $[\text{Mn}(\text{pmt})_2(\text{o-phen})]$ (**1**) and $[\text{Zn}(\text{pmt})_2(\text{o-phen})]$ (**2**) derived from 4-phenyl(2-methoxybenzoyl)-3-thiosemicarbazide (Hpmt) containing *o*-phen as coligand. TGA show that the complexes are stable up to 200 °C, indicating the absence of lattice water as well as coordinated water and finally $\text{Mn}(\text{NCO})_2$ and $\text{Zn}(\text{NCSNH})_2$ are obtained as the residue. The optimized energy of Hpmt and complexes are -905.290 (Hpmt), -2484.971 $\{[\text{Mn}(\text{pmt})_2(\text{o-phen})]\}$ and -2446.640 $\{[\text{Zn}(\text{pmt})_2(\text{o-phen})]\}$ a.u., respectively. MEP map and contour plot of Hpmt show that the metal ions preferably bind through the carbonyl oxygen and hydrazine nitrogen forming a stable five membered chelate ring. The small HOMO–LUMO energy gap for the Zn(II) complex suggests low excitation energy for $\pi \rightarrow \pi^*$ and $n \rightarrow \pi^*$ transitions than the Mn(II) complex and the same is supported by the UV–Vis spectral data. The crystal structure of complexes **1** and **2** are stabilized through weak intramolecular $\text{N-H} \cdots \text{O}$, $\text{N-H} \cdots \text{S}$ and $\text{C-H} \cdots \text{S}$ interactions producing supramolecular architecture. Results obtained from Density Functional Theory calculation corroborate our experimental findings from X-ray.

Appendix A. Supplementary data

CCDC 916920 and 916921 contain the supplementary crystallographic data for $[\text{Mn}(\text{pmt})_2(\text{o-phen})]$ (**1**) and $[\text{Zn}(\text{pmt})_2(\text{o-phen})]$ (**2**), respectively. These data can be obtained free of charge via <http://www.ccdc.cam.ac.uk/conts/retrieving.html>, or from the Cambridge Crystallographic Data center, 12 Union Road,

Cambridge CB2 1EZ, UK; fax: (+44)1223-336-033; or e-mail: deposit@ccdc.cam.ac.uk.

References

- [1] K. Zamani, K. Faghihi, M.R. Sangi, J. Zolgharnein, *Turk. J. Chem.* 27 (2003) 119.
- [2] R.M. Shaker, A.F. Mahmoud, F.F. Abdel-Latif, *Phosphorus, Sulfur Silicon* 180 (2005) 397.
- [3] T.R. Hovsepian, E.R. Dilanian, A.P. Engoyan, R.G. Melik-Ohanjanian, *Chem. Heterocycl. Compd.* 40 (2004) 9.
- [4] J.P. Scroville, D.L. Klayman, C.F. Franchino, *J. Med. Chem.* 25 (1982) 1261.
- [5] D.X. West, C.S. Carlson, A.E. Liberta, J.P. Scroville, *Transition Met. Chem.* 15 (1991) 383.
- [6] D.X. West, N.M. Kozub, G.A. Bain, *Transition Met. Chem.* 21 (1996) 52.
- [7] D.X. West, M.M. Salberg, G.A. Bain, A.E. Liberta, *Transition Met. Chem.* 22 (1997) 180.
- [8] K. Raman, H.K. Singh, S.K. Salzman, S.S. Parmar, *J. Pharm. Sci.* 82 (1993) 167.
- [9] M.C. Cardiaa, S. Distinto, E. Maccioni, A. Plumitallo, M. Saggi, M.L. Sanna, A. DeLogu, *J. Heterocycl. Chem.* 43 (2006) 1337.
- [10] G. Küçüküzgel, A. Kocatepe, E. De Clercq, F. Şahin, M. Güllüce, *Eur. J. Med. Chem.* 41 (2006) 353.
- [11] T. Plech, M. Wujec, A. Siwek, U. Kosikowska, A. Malm, *Eur. J. Med. Chem.* 46 (2011) 241.
- [12] N. Ulusoy, N. Ergenc, G.O. Saniş, *Acta Pharm Turcica.* 38 (1996) 111.
- [13] H.N. Doğan, S. Rollas, H. Erdeniz, *Farmaco* 53 (1998) 462.
- [14] I. Kerimov, G. Ayhan-Kilçigil, B. Can-Eke, N. Altanlar, M. İscan, *J. Enzyme Inhib. Med. Chem.* 22 (2007) 696.
- [15] A. Siwek, P. Staczek, J. Stefanska, *Eur. J. Med. Chem.* 46 (2011) 5717.
- [16] S.A. Mayekar, V.V. Mulwad, *Ind. J. Chem.* 47B (2008) 1438.
- [17] V. Amani, N. Safari, H.R. Khavasi, P. Mirzaei, *Polyhedron* 26 (2007) 4908.
- [18] L.G. Bachas, L. Cullen, R.S. Hutchins, D.L. Scott, *J. Chem. Soc., Dalton Trans.* (1997) 1571.
- [19] C.S. Chow, F.M. Bogdan, *Chem. Rev.* 97 (1997) 1489.
- [20] F. Calderazzo, G. Pampaloni, V. Passarelli, *Inorg. Chim. Acta* 330 (2002) 136.
- [21] J.W. Steed, J.L. Atwood, *Supramolecular Chemistry*, Wiley, Chichester, 2000.
- [22] K. Binnemans, P. Lenaerts, K. Driesen, C. Görller-Walrand, *J. Mater. Chem.* 14 (2004) 191.
- [23] P. Lenaerts, A. Storms, J. Mullens, J. D'Haen, C. Görller-Walrand, K. Binnemans, K. Driesen, *Chem. Mater.* 17 (2005) 5194.

- [24] P.N. Hawker, M.V. Twigg, in: G. Wilkinson, R.D. Gillard, J.A. McCleverty (Eds.), *Comprehensive Coordination Chemistry*, vol. 4, Pergamon press, Oxford, 1987.
- [25] H.G. Petering, H.H. Buskik, G.E. Underwood, *Cancer Res.* 64 (1964) 367.
- [26] A. EL-Asmy, A. Mostafa, *Polyhedron* 2 (1983) 591.
- [27] K.M. Khan, M. Rasheed, Z. Ullah, S. Hayat, F. Kaukab, M.I. Choudhary, A. Rahman, S. Perveen, *Bioorg. Med. Chem.* 11 (2003) 1381.
- [28] G.M. Sheldrick, *Acta Cryst. A* 64 (2008) 112.
- [29] I.J. Bruno, J.C. Cole, P.R. Edgington, M. Kessler, C.F. Macrae, P. McCabe, J. Pearson, R. Taylor, *Acta Crystallogr., Sect. B* 58 (2002) 389.
- [30] L.J. Farrugia, *J. Appl. Crystallogr.* 30 (1997) 565.
- [31] Q.Q. Jian, B. Darhkijav, H. Liu, J. Wang, Z. Li, B. Jianh, *Chem. Asian J.* 5 (2010) 543.
- [32] K. Nakamoto, *Infrared and Raman Spectra of Inorganic and Coordination Compounds*, fourth ed., Wiley Interscience, New York, 1986.
- [33] A.B.P. Lever, *Inorganic Electronic Spectroscopy*, second ed., Elsevier, Amsterdam, 1984.
- [34] G. Pelosi, *Open Crystallogr. J.* 3 (2010) 16.
- [35] M.X. Li, C.L. Chen, D. Zhang, J.Y. Niu, B.S. Ji, *Eur. J. Med. Chem.* 45 (2010) 3169.
- [36] M.J. Frisch, G.W. Trucks, H.B. Schlegel, G.E. Scuseria, M.A. Robb, J.R. Cheeseman, V.G. Zakrzewski, J.A. Montgomery, Jr.R.E. Stratmann, J.C. Burant, S. Dapprich, J.M. Millam, A.D. Daniels, K.N. Kudin, M.C. Strain, O. Farkas, J.B. V. Tomasi, M. Cossi, R. Cammi, B. Mennucci, C. Pomelli, C. Adamo, S. Clifford, J. Ochterski, G.A. Petersson, P.Y. Ayala, Q. Cui, D.K. Morokuma, A.D. Malick, K. Rabuck, J.B. Raghavachari, J. Foresman, J. Cioslowski, J.V. Ortiz, A.G. Baboul, B.B. Stefanov, G.L.A. Liu, P. Piskorz, I. Komaromi, R. Gomperts, R.L. Martin, D.J. Fox, T. Keith, M.A. Al-Laham, C.Y. Peng, A. Nanayakkara, M. Challacombe, P.M.W. Gill, B.Johnson, W. Chen, M.W. Wong, J.L. Andres, C. Gonzalez, M. Head-Gordon, E.S. Replogle, J.A. Pople, *GAUSSIAN 03*, Revision A.1, Gaussian Inc, Pittsburgh, 2003.
- [37] A.D. Becke, *J. Chem. Phys.* 98 (1993) 5648.
- [38] C. Lee, W. Yang, R.G. Parr, *Phys. Rev. B.* 37 (1988) 785.
- [39] K. Fukui, *Science* 218 (1982) 747.